Mechanical Analysis of Elastomer Seal in Subsea Pipeline Plugging Robot

Wang Mingkuan[1], Zhang Enchao[1], Zhang Shimin[1, 2], Zhu Xiaoxiao[3, 4, *]

[1]College of Mechanical and Transportation Engineering, China University of Petroleum (Beijing), Beijing 102249, China
[2]College of Engineering, Karamay Campus, China University of Petroleum (Beijing), Karamay 834000, China
[3]College of Safety and Ocean Engineering, China University of Petroleum (Beijing), Beijing 102249, China
[4]Key Laboratory of Oil and Gas Production Safety and Emergency Technology, Ministry of Emergency Management, Beijing 102249, China

Abstract: To address the urgent demands of emergency repair following subsea pipeline leaks, pipeline isolation technology has emerged as a key development direction for subsea intervention systems. As the core functional component of subsea pipeline plugging robot, elastomer seal plays a critical role in both setting reliability and sealing performance. This study first reviews the typical operational workflow of subsea pipeline plugging robot and elucidates the “self energisation” mechanism of elastomer seal under high-pressure internal fluids. On this basis, a mechanical model of elastomer seal is formulated, and a theoretical expression for the contact stress between Elastomer seal and the pipe wall was derived. Five commonly used hyperelastic constitutive models are then examined, and their strain-energy functions and engineering stress expressions under uniaxial tension are systematically derived to provide a theoretical basis for rubber-material parameter identification. Subsequently, numerical simulations of elastomer seal’s sealing behavior under the hydraulic actuation system are performed in ABAQUS, followed by pressure-penetration-based analyses of the contact stress distribution under the combined action of the setting load and internal fluid pressure. Comparison between theoretical predictions and finite-element results enables further refinement of the contact stress formula, allowing the corrected model to more accurately predict elastomer seal sealing performance under hydraulic driving. The findings provide a reliable analytical framework to support the structural optimization and engineering design of subsea pipeline isolation devices.

Keywords: Subsea Pipeline Plugging Robot; Elastomer Seal; Sealing Performance; Pressure-Penetration Method

DOI: 10.57237/j.mse.2026.01.001

1 Introduction

China’s long-distance oil and gas pipeline network now exceeds 180,000 km, with pipelines that have been in service for more than 20 years accounting for approximately 20%–30% of the total. As these aging pipelines experience progressive corrosion and structural degradation, the likelihood of leakage events increases markedly [1]. For both offshore and onshore systems, traditional emergency repair approaches primarily rely on hot tapping & line plugging pipeline isolation [2]. However, these methods exhibit inherent limitations, including low allowable sealing pressure, reduced sealing reliability, and the unavoidable generation of branch-connection scars, all of which compromise long-term operational safety. To overcome these challenges, pipeline plugging robot technology has emerged as a promising alternative. By deploying advanced pipeline plugging robot inside pipelines [3, 4] and enabling real-

Funding: This work was supported by the National Key Research and Development Program of China (Serial number: 2022YFC2806103).

*Corresponding author: Zhu Xiaoxiao, x.zhu@cup.edu.cn

Received: 25 February 2026; Accepted: 7 March 2026; Published Online: 12 March 2026 http://www.mechscieng.com

time communication between pipeline plugging robot and the external control system, leakage defects can be repaired internally without requiring intrusive external operations on the pipeline structure.

Currently, pipeline isolation plugging technology is primarily mastered by foreign oilfield service companies. The SmartPlug system developed by TDW (USA), is applicable to both onshore and subsea pipelines ranging from 10" to 42" in diameter, and can withstand a maximum plugging pressure of 20 MPa [5]. StatsGroup in the United Kingdom has also made significant advances in intelligent pipeline isolation tools in recent years. Its TecnoPlug system [6], is designed for pipelines from 3" to 42" and achieves plugging pressures of up to 35 MPa. The structure and operating principle of TecnoPlug are largely similar to those of SmartPlug; However, the TecnoPlug integrates two sealing rubber sleeves into a single unit, enabling simultaneous seal verification while significantly reducing the overall tool size.

The pipeline plugging robot serves as the carrier for implementing in-pipe plugging technology, within which elastomer seal functions as the core component. Its primary roles are to establish a reliable seal, isolate internal oil and gas, and protect pipeline integrity. Therefore, enhancing the sealing performance of elastomer seal is essential for meeting the increasingly high pressure demands of modern oil and gas pipelines. To elucidate the sealing behavior and mechanical characteristics of elastomer seals, extensive research has been conducted both in China and abroad. Zhang et al. optimized packer rubber cartridges using an orthogonal design approach and quantified the effects of structural parameters on sealing performance [7]. Li et al. improved contact stress by introducing a wavy cartridge geometry [8], while Huang et al. proposed a novel structure that reduces shoulder extrusion and enhances sealing reliability [9]. Zhang Kang et al. optimized intelligent plugging cartridges using single- and multi-factor coupling analyses and identified parameter combinations that maximize contact stress under a given driving force [10]. Xu Jing et al. introduced an effective sealing coefficient to evaluate packer performance and examined the influences of hardness and friction coefficient [11]. Hu et al. investigated the sealing behavior of compression-type packer elements through combined simulations and experiments [12], and Sun Qiaolei et al. analyzed the effects of annular pressure and chamfer geometry on cartridge sealing performance [13]. Chen et al. developed a mathematical model for FKM-based packer elements suitable for high-temperature, high-pressure environments [14]. Wang et al. examined the role of friction coefficient and improved packer design by regulating contact friction [15], while He et al. clarified the effects of axial loading and elevated temperature on sealing behavior [16]. Polonsky et al. enhanced sealing integrity by redesigning cylindrical cartridges into conical forms reinforced with anti-extrusion helical springs [17]. Zhu et al. established a supercritical CO_2 penetration–deformation model for rubber cartridges [18], and Li et al. introduced a spring-reinforced shoulder-protection structure to mitigate extrusion failure [19]. Zhang et al. significantly improved the performance of nylon-cord expansion packers for low-permeability reservoirs through structural optimization [20]. Fei et al. proposed a fluid–structure interaction leakage model capable of accurately predicting performance under high-temperature, high-pressure conditions and quantified the effects of cartridge number and length [21]. Song et al. combined full factorial DOE with finite-element simulations to identify optimal structural parameters for rubber packers [22], and Li et al. developed a temperature–pressure-coupled mechanical model and failure evaluation framework for reliability assessment in deep-water HPHT gas wells [23]. Although these studies provide valuable insights into the mechanical behavior and, in some cases, the structural optimization of packer sealing elements, packer cartridges generally operate under relatively small deformation and differ substantially from the large-deformation, large-diameter elastomer seal used in subsea pipeline plugging robot. Research on these elastomer seal must consider the nonlinear hyperelastic behavior of rubber, complex geometries, significant deformation under axial loading, and the effects of high-pressure internal fluids. Furthermore, theoretical derivations of elastomer seal–pipe-wall contact stress distribution and investigations into the "self energisation" mechanism unique to subsea pipeline plugging robot remain largely underexplored.

Therefore, this study first elastomer seal a mechanical model of elastomer seal and derives the theoretical expression for the contact stress between elastomer seal and the pipe wall. The strain-energy functions and nominal stress formulations under uniaxial tension for several hyperelastic models are systematically presented, on the basis of which the optimal constitutive model for representing the rubber's mechanical response is identified. Subsequently, ABAQUS is employed to simulate the sealing performance of elastomer seal under the setting load, and the pressure-penetration method is incorporated to analyze the contact stress distribution under the combined effects of the setting load and internal fluid pressure. By comparing theoretical predictions with numerical results, the contact stress model is further refined, allowing the corrected formulation to more accurately predict elastomer seal–pipe contact stress under hydraulic actuation. The findings provide a robust theoretical foundation and analytical framework for the structural optimization and engineering design of subsea in-pipe plugging devices.

2 Working Principle of the Subsea Pipeline Plugging Robot

2.1 Operational Workflow of the Subsea Pipeline Plugging Robot

When a leak occurs in a subsea pipeline, intelligent in-pipe plugging technology can be employed as an emergency response. Two sets of plugging robots are deployed from the offshore platform's launch unit and inserted into the pipeline. Using precise positioning and volumetric measurement techniques, the robots are guided to predetermined locations upstream and downstream of the leakage point. Operators on the vessel or platform then transmit commands through an acoustic communication system. The underwater receiving unit couples with the external communication module and converts the acoustic signals into ultra-low-frequency electromagnetic pulses, which can propagate through the metallic pipe wall, as illustrated in Figure 1.

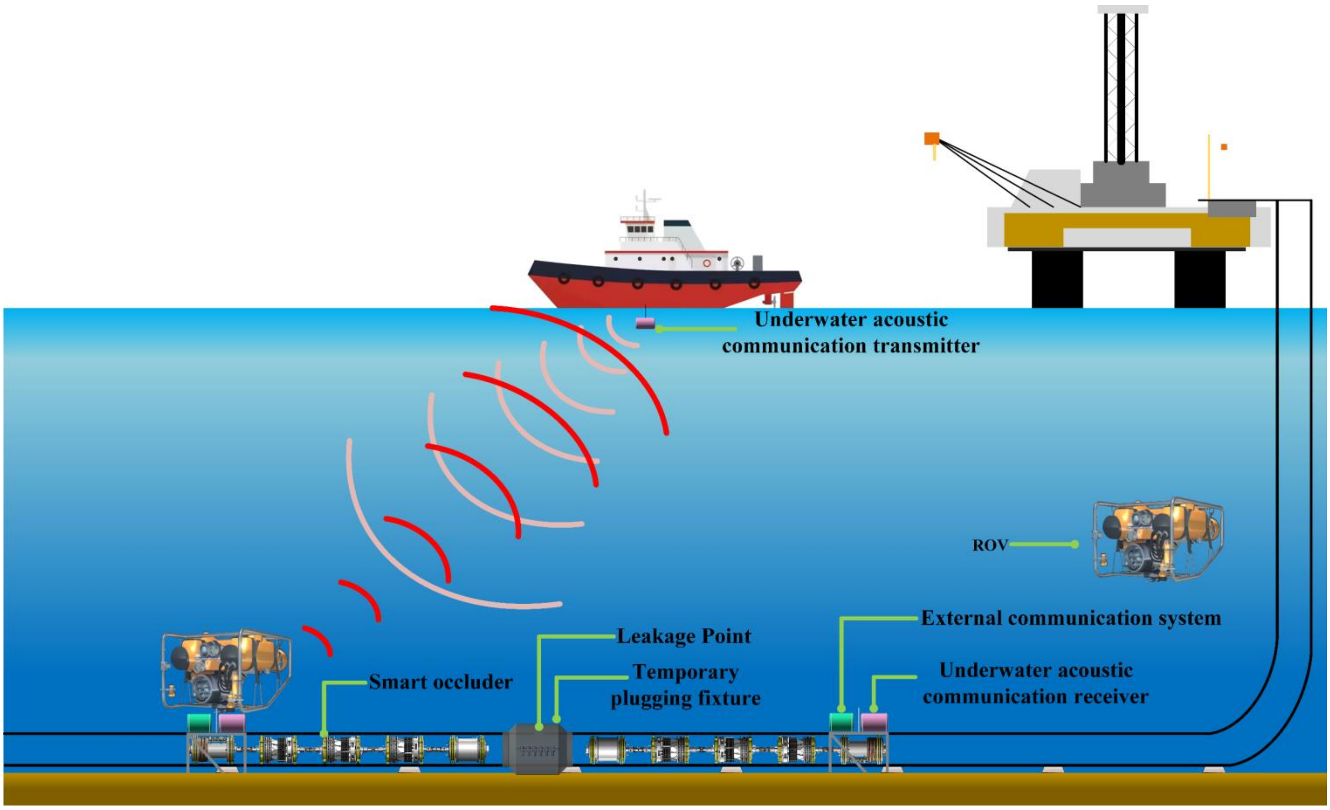

Figure 1 Acoustic and In-Pipe/Out-of-Pipe Communication Flowchart of the Pipeline Plugging Robot

After bidirectional communication between the inside and outside of the pipeline is established, operational commands remotely activate the internal control system of the plugging robot. The robot is equipped with three sealing units, each consisting of a hydraulic cylinder. These cylinders operate in parallel and in coordination, and their three-dimensional structure is shown in Figure 2. Upon receiving a control signal, the hydraulic cylinders first actuate the anchoring mechanism, driving the slips along the inclined surfaces until they firmly engage the pipe wall, thereby completing the anchoring process. The cylinders then continue to advance the frame, compressing elastomer seal and inducing radial expansion. This expansion enables tight, high-pressure contact with the pipe wall, forming an effective barrier against the internal fluid. Once sealing is achieved, the downstream pressure is reduced. The remaining internal pressure increases the normal contact force between the slips and the pipe wall while simultaneously driving the frame to compress the cartridge further. This enhances the contact stress and strengthens the sealing performance, ensuring reliable isolation of the pipeline medium at the damaged section. After the repair operation is completed, the communication system issues a command to activate the hydraulic release circuit. The cylinders then retract simultaneously, disengaging both the slips and the expanded cartridge. Finally, driven by the pipeline pressure, the plugging robot travels along the pipe and is retrieved into the receiving barrel, ensuring safe recovery.

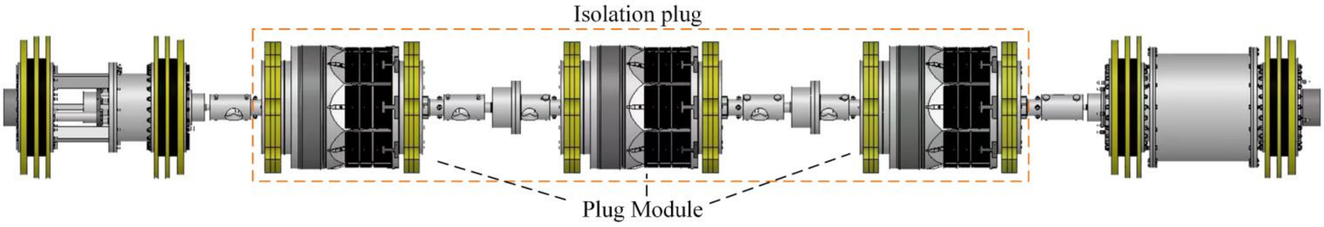

Figure 2 Three-Dimensional structural diagram of the subsea pipeline plugging robot

2.2 Self Energisation Mechanism of Elastomer Seal in the Subsea Pipeline Plugging Robot

After the subsea pipeline plugging robot completes the setting process under the action of the hydraulic system, the upstream internal fluid pressure begins to act on elastomer seal. Driven by the pressure differential, the cartridge undergoes increasing radial compression, exhibiting a characteristic "the higher the pressure, the tighter the seal" behavior. As a result, the contact stress between elastomer seal and the pipe wall continually increases, thereby achieving an effective sealing state. Based on this principle, once an initial seal is established, the internal medium can be reliably isolated. This phenomenon is referred to as the self energisation characteristic of elastomer seal.

3 Theoretical Formulation of the Contact Stress for Elastomer Seal

In this study, the contact stress between elastomer seal and the pipe wall is first derived for the condition in which the cartridge has completed the setting process under hydraulic actuation. ABAQUS, combined with the pressure-penetration method, is subsequently employed to simulate the variation in contact stress under different isolated pressure. The operating principle of the plug module in the subsea pipeline plugging robot is illustrated in Figure 3. Under the axial driving load F_z generated by hydraulic actuation, elastomer seal undergoes axial compression, which induces radial expansion. During this expansion process, Elastomer seal gradually contacts the inner wall of the pipe and develops a contact pressure P_c.

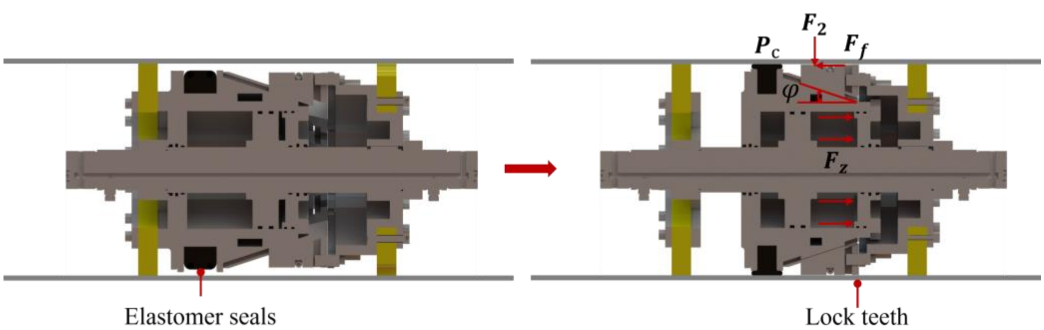

Figure 3 Operating Principle of the Plug Module

Assuming that elastomer seal, when subjected to an axial compression force F_z, generates a contact pressure P_c against the pipe wall, the condition for achieving internal-pressure sealing is that the sealing capacity of elastomer seal must exceed the pressure differential across its two ends. Because elastomer seal and the lock teeth are integrated into the same structural assembly, the axial force induced by the internal pressure differential is entirely borne by the lock teeth. Consequently, the primary function of elastomer seal is to provide localized sealing rather than sustaining the global axial load. Based on this analysis, the contact pressure between elastomer seal and the pipe wall can be regarded as the effective sealing capacity of elastomer seal. Therefore, the condition for successful sealing by elastomer seal in the pipeline plugging robot can be expressed as:

$$P_c > \Delta P, F_f > F_z \tag{1}$$

where P_c is the contact pressure between elastomer seal and the pipe wall (MPa); ΔP is the isolated pressure (MPa); F_f is the frictional force generated between the lock teeth and the pipe wall (N); and F_z is the thrust induced by the pressure differential acting on both ends of the pipeline plugging robot (N).

3.1 Plug-Setting Stage

Analysis shows that the deformation of elastomer seal during compression and its gradual contact with the pipe wall can be divided into two distinct stages. In the first stage, elastomer seal undergoes axial compression and radial expansion under the applied load, but it has not yet reached the pipe wall; this stage is characterized by free radial expansion. Once the cartridge contacts the pipe wall, the second stage begins. In this stage, further increases in axial compressive load no longer produce additional radial expansion because the pipe wall imposes a geometric constraint. Instead, the contact pressure between Elastomer seal and the pipe wall continues to increase.

Although elastomer seal undergoes axial compressive deformation, it remains unconstrained in the radial direction. The differential equation governing its radial displacement is:

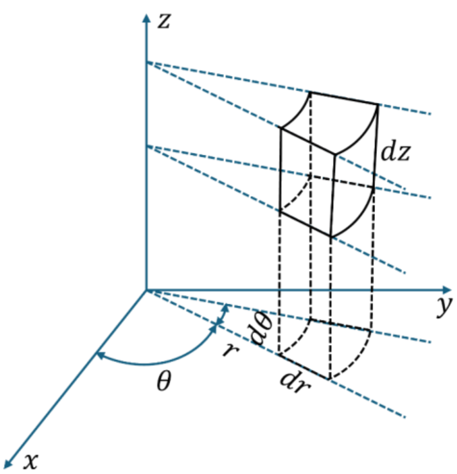

Figure 4 Cylindrical Coordinate System

$$\frac{d^2u}{dr^2} + \frac{1}{r}\frac{du}{dr} - \frac{u}{r^2} = 0 \tag{2}$$

The general solution can be expressed as:

$$u = Ar + \frac{B}{r} \tag{3}$$

Where, u denotes the radial displacement and r represents the radius of curvature.

The boundary conditions can be expressed as:

$$\begin{cases} u_r \mid_{r=R_1} = 0 \\ u_r \mid_{r=R_3} = R_3 - R_2 \end{cases} \tag{4}$$

Where, R_1 denotes the inner diameter of elastomer seal; R_2 denotes the outer diameter of elastomer seal; R_3 denotes the inner diameter of the subsea pipeline.

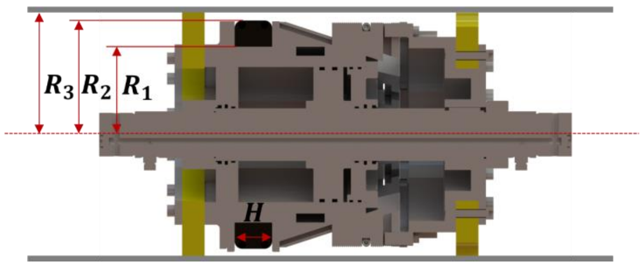

Figure 5 Schematic Diagram of the Geometric Dimensions

Eq. (4) was substituted into Eq. (3) to obtain:

$$A = \frac{(R_3 - R_2)R_3}{R_3^2 - R_1^2}, B = -\frac{(R_3 - R_2)R_1^2 R_3}{R_3^2 - R_1^2} \tag{5}$$

By applying the geometric relations for axisymmetric deformation, the relative radial strain ε_r and the relative circumferential strain ε_θ can be expressed as follows:

$$\varepsilon_r = \frac{du}{dr} = \frac{(R_3 - R_2)R_3}{R_3^2 - R_1^2} + \frac{(R_3 - R_2)R_1^2 R_3}{r^2\left(R_3^2 - R_1^2\right)} \tag{6}$$

$$\varepsilon_\theta = \frac{u}{r} = \frac{(R_3 - R_2)R_3}{R_3^2 - R_1^2} - \frac{(R_3 - R_2)R_1^2 R_3}{r^2\left(R_3^2 - R_1^2\right)} \tag{7}$$

Based on the assumption of volume incompressibility before and after the deformation of elastomer seal in the subsea pipeline plugging robot, the condition $\varepsilon_r + \varepsilon_\theta + \varepsilon_z = 0$ must be satisfied. Therefore:

$$\varepsilon_z = -\left(\varepsilon_r + \varepsilon_\theta\right) = -\frac{2R_3\left(R_3 - R_2\right)}{R_3^2 - R_1^2} \tag{8}$$

Where, the negative sign indicates that ε_z is in a state of compression.

When elastomer seal is subjected to the setting load provided by the hydraulic actuation system, the compression ratio η of elastomer seal is introduced. According to elastic mechanics theory, once elastomer seal comes into contact with the inner wall of the pipeline, the relationship between the post-deformation compression ratio and the resulting compressive strain can be expressed as follows:

$$\eta = 1 - \varepsilon \tag{9}$$

$$\eta = \frac{H_1}{H} = 1 - \frac{2R_3\left(R_3 - R_2\right)}{R_3^2 - R_1^2} \tag{10}$$

Where, η denotes the compression ratio; H denotes the original height of elastomer seal; and H_1 denotes the height of elastomer seal at the moment when initial sealing with the pipeline is achieved.

According to the principles of statics, the axial stress σ_{z1} of elastomer seal during the free-deformation stage is related to the compression ratio η, and can be expressed as:

$$\sigma_{z1} = G\left(\frac{1}{\eta} - \eta^2\right) \tag{11}$$

Where, G denotes the shear modulus, $G = \frac{E}{2(1+\mu)}$.

From Eq. (11), the axial stress σ_{z1} of elastomer seal in the free-deformation stage can be expressed as follows:

$$\sigma_{z1} = \frac{E\left[\left(R_3^2 - R_1^2\right)^3 - \left(R_2^2 - R_1^2\right)^3\right]}{2(1+\mu)\left(R_2^2 - R_1^2\right)\left(R_3^2 - R_1^2\right)^2} \tag{12}$$

After elastomer seal completes the setting process under the load applied by the hydraulic actuation system, the resulting axial stress can be expressed as:

$$\sigma_z = \frac{F_z}{S} = \sigma_{z1} + \sigma_{z2} \tag{13}$$

Where, σ_{z1}, σ_{z2} denote the axial stresses of elastomer seal during the free-deformation stage and the constrained-deformation stage, respectively; F_z denotes axial compressive force provided by the hydraulic actuation system; and S denotes the cross-sectional area of elastomer seal in its deformed state.

According to the generalized Hooke's law, elastomer seal undergoes axial compression during the free-deformation stage. The constitutive relations for the radial, circumferential, and axial stress components can be expressed as follows:

$$\sigma_r = \frac{E}{(1-2\mu)(1+\mu)}\left[(1-\mu)\varepsilon_r + \mu\left(\varepsilon_\theta + \varepsilon_z\right)\right] \tag{14}$$

$$\sigma_{z2} = \frac{E}{(1-2\mu)(1+\mu)}\left[(1-\mu)\varepsilon_z + \mu\left(\varepsilon_r + \varepsilon_\theta\right)\right] \tag{15}$$

During the constrained-deformation stage, elastomer seal comes into contact with the pipe wall and is constrained in both the axial and radial directions. Because the stiffness of the pipe and other metal components is significantly greater than that of elastomer seal, the radial and circumferential deformations satisfy $\varepsilon_r = \varepsilon_\theta = 0$. Therefore:

$$\frac{\sigma_r}{\sigma_{z2}} = \frac{\mu}{1-\mu} \tag{16}$$

Where, σ_r denotes the radial stress acting on elastomer seal and μ denotes Poisson's ratio.

From the above relations, it follows that:

$$\sigma_r = \frac{\mu}{1-\mu}\sigma_{z2} \tag{17}$$

From Eq. (13), we obtain:

$$\sigma_{z2} = \frac{F_z}{S} - G\left(\frac{1}{\eta} - \eta^2\right) \tag{18}$$

Substituting Eq. (10) into Eq. (18) yields:

$$P_{c1} = \sigma_r = \frac{\mu}{1-\mu}\left[\frac{F_z}{S} - G\left(\frac{1}{\eta} - \eta^2\right)\right] = \frac{\mu}{1-\mu}\left\{\frac{F_z}{\pi\left(R_3^2 - R_1^2\right)} - \frac{E\left[\left(R_3^2 - R_1^2\right)^3 - \left(R_2^2 - R_1^2\right)^3\right]}{2(1+\mu)\left(R_2^2 - R_1^2\right)\left(R_3^2 - R_1^2\right)^2}\right\} \tag{19}$$

3.2 Plugging Stage

After elastomer seal completes the setting process, it continues to develop axial stress under the applied pressure differential ΔP. This axial stress is carried by the sealing element and is balanced by the resulting shear stress τ_{rz} within elastomer seal.

$$2\pi\tau_{rz}R_3L = \pi\left(R_3^2 - R_1^2\right)\Delta P \tag{20}$$

$$\tau_{rz} = \frac{\Delta P\left(R_3^2 - R_1^2\right)}{2R_3L} \tag{21}$$

Where, L denotes the contact length between elastomer seal and the pipe wall (mm).

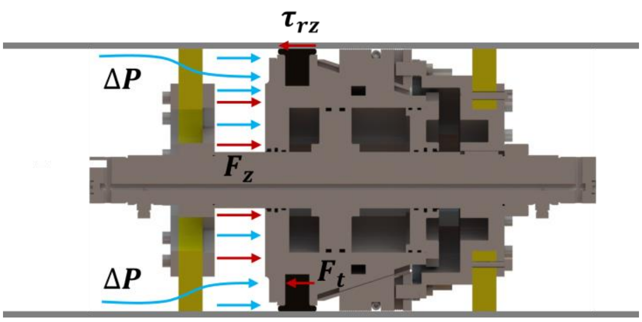

Figure 6 Schematic Diagram of the Loading Conditions During the Plugging Stage

To evaluate the influence of shear deformation on the sealing performance of the subsea pipeline plugging robot, the relationship between shear stress and axial stress can be determined using the general elastic theory for incompressible materials. A schematic diagram of the loading conditions during the plugging stage of the pipeline plugging robot is shown in Figure 6.

$$\frac{\partial\sigma_z}{\partial z} - \frac{\partial\tau_{rz}}{\partial r} - \frac{\partial\tau_{z\theta}}{\partial\theta} = 0 \tag{22}$$

Under the conditions $\varepsilon_r = \varepsilon_\theta = 0$ and $\tau_{z\theta} = \tau_{r\theta} = 0$, From equation (22), we can obtain:

$$\frac{\partial\sigma_z}{\partial z} = -\frac{\partial\tau_{rz}}{\partial r} \tag{23}$$

From Eq. (21), it can be seen that the shear stress τ_{rz} is a function of the two variables R_3 and R_1. Differentiating with respect to these variables yields:

$$\frac{\partial\tau_{rz}}{\partial r} = \frac{\Delta P}{2L}\left(\frac{R_3 - R_1}{R_3}\right)^2 \tag{24}$$

Therefore:

$$\frac{\partial\sigma_z}{\partial z} = -\frac{\Delta P}{2L}\left(\frac{R_3 - R_1}{R_3}\right)^2 \tag{25}$$

Thus:

$$\sigma_z = \Delta P - \frac{z\Delta P}{2L}\left(\frac{R_3 - R_1}{R_3}\right)^2 \tag{26}$$

Where, z denotes the contact length at the section.

Substituting equation (26) into $\sigma_r = \frac{\mu}{1-\mu}\sigma_z$, we get the contact pressure between elastomer seal and the pipe wall under the applied differential isolated pressure can be expressed as:

$$P_{c2} = \sigma_r = \frac{\mu\Delta P}{1-\mu}\left[1 - \frac{z}{2L}\left(\frac{R_3 - R_1}{R_3}\right)^2\right] \tag{27}$$

Thus, the total contact pressure at this stage can be expressed as:

$$P = \frac{\mu}{1-\mu}\left\{\frac{F_z}{\pi\left(R_3^2 - R_1^2\right)} - \frac{E\left[\left(R_3^2 - R_1^2\right)^3 - \left(R_2^2 - R_1^2\right)^3\right]}{2(1+\mu)\left(R_2^2 - R_1^2\right)\left(R_3^2 - R_1^2\right)^2}\right\} + \frac{\mu\Delta P}{1-\mu}\left[1 - \frac{z}{2L}\left(\frac{R_3 - R_1}{R_3}\right)^2\right] \tag{28}$$

4 Study on the Sealing Performance of Elastomer Seal Based on ABAQUS

4.1 Principle of the Pressure-Penetration Method in ABAQUS

According to the ABAQUS Theory Manual [24], fluid pressure penetration in the ABAQUS/Standard module is simulated by defining the starting point of a "master–slave" penetration pair. From this point onward, the fluid pressure propagates along the contact interface, and the applied pressure always acts normal to the surface. During the penetration process, penetration ceases at any node where the contact pressure exceeds the applied fluid pressure, causing the fluid front to remain at that node, as illustrated in Figure 7. This loading strategy automatically identifies the critical location where fluid penetration induces separation at the contact interface, thereby enabling a more accurate assessment of the sealing performance of elastomer seal.

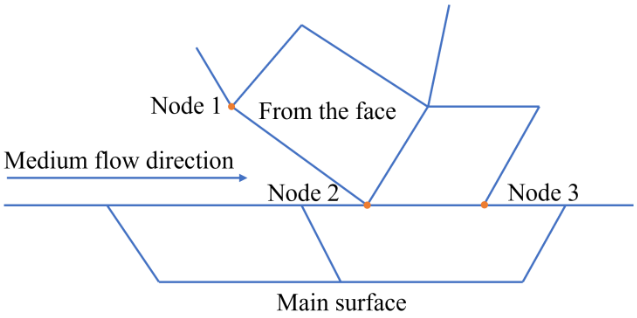

Figure 7 Application of Fluid Pressure–Penetration Loading

4.2 Numerical Simulation Model

4.2.1 Study on Rubber Constitutive Models

To accurately characterize the large-deformation mechanical behavior of the rubber material, uniaxial tensile tests were conducted in this study. The stress–strain responses obtained at different strain levels provide the experimental basis for subsequent identification of the constitutive model parameters. The experimental setup is illustrated in Figure 8.

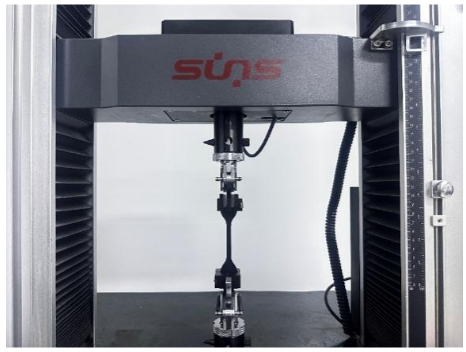

Figure 8 Uniaxial Tensile Test

4.2.2 Common Hyperelastic Constitutive Models

(i) Mooney-Rivlin Model [25]

The strain energy density function can be expressed as:

$$W = C_{10}(\bar{I}_1 - 3) + C_{01}(\bar{I}_2 - 3) \tag{29}$$

where C_{10}, C_{01} denotes the unknown material parameters.

The nominal stress–strain relationship can be expressed as:

$$\sigma = \frac{\partial W}{\partial \lambda_U} = \frac{\partial W}{\partial \bar{I}_1}\frac{\partial \bar{I}_1}{\partial \lambda_U} + \frac{\partial W}{\partial \bar{I}_2}\frac{\partial \bar{I}_2}{\partial \lambda_U} = 2\left(1-\lambda_U^{-3}\right)\left(C_{10}\lambda_U + C_{01}\right) \tag{30}$$

(ii) Ogden Model [26]

The strain energy density function can be expressed as:

$$W = \sum_{i=1}^{N}\frac{2\mu_i}{\alpha_i^2}\left(\lambda_1^{\alpha_i} + \lambda_2^{\alpha_i} + \lambda_3^{\alpha_i} - 3\right) \tag{31}$$

where μ_i, α_i denotes the unknown material parameters, and λ_i denotes the principal stretch.

The nominal stress–strain relationship can be expressed as:

$$\sigma = \frac{\partial W}{\partial \lambda_U} = \sum_{i=1}^{N}\frac{2\mu_i}{\alpha_i}\left(\lambda^{\alpha_i - 1} - \lambda^{-\frac{1}{2}\alpha_i - 1}\right) \tag{32}$$

(iii) Yeoh Model [27]

The strain energy density function can be expressed as:

$$W = \sum_{i=1}^{3} C_{i0}(\bar{I}_1 - 3)^i \tag{33}$$

Where, C_{i0} denotes the unknown material parameters.

The nominal stress–strain relationship can be expressed as:

$$\sigma = \frac{\partial W}{\partial \lambda_U} = \frac{\partial W}{\partial \bar{I}_1}\frac{\partial \bar{I}_1}{\partial \lambda_U} + \frac{\partial W}{\partial \bar{I}_2}\frac{\partial \bar{I}_2}{\partial \lambda_U} = 2(\lambda_U - \lambda_U^{-2})C_{10} + 4(\lambda_U^3 - 3\lambda_U + 3\lambda_U^{-2} - 2\lambda_U^{-3} + 1)C_{20} + 6(\lambda_U^2 + 2\lambda_U^{-1} - 3)^2(\lambda_U - \lambda_U^{-2})C_{30} \tag{34}$$

(iv) Arruda-Boyce Model [28]

The strain energy density function can be expressed as:

$$W = \mu\sum_{i=1}^{5}\frac{C_i}{\lambda_m^{2i-2}}(\bar{I}_1^i - 3^i) \tag{35}$$

Where, μ, λ_m denotes the unknown material parameters.

The nominal stress–strain relationship can be expressed as:

$$\sigma = \frac{\partial W}{\partial \lambda_U} = 2\mu(\lambda_U - \lambda_U^{-2})\sum_{i=1}^{5}\frac{iC_i}{\lambda_m^{2i-2}}\bar{I}_1^{i-1} \tag{36}$$

(v) Neo-Hookean Model [29]

The strain energy density function can be expressed as:

$$W = C_{10}\left(\bar{I}_1 - 3\right) \tag{37}$$

Where, C_{10} denotes the unknown material parameters.

The nominal stress–strain relationship can be expressed as:

$$\sigma = \frac{\partial W}{\partial \lambda_U} = \frac{\partial W}{\partial \bar{I}_1}\frac{\partial \bar{I}_1}{\partial \lambda_U} + \frac{\partial W}{\partial \bar{I}_2}\frac{\partial \bar{I}_2}{\partial \lambda_U} = 2C_{10}\left(\lambda_U - \lambda_U^{-2}\right) \tag{38}$$

4.2.3 Analysis of Fitting Results

Because elastomer seal is made of hydrogenated nitrile rubber (HNBR), a material with excessively low hardness may undergo outward bulging after compression, thereby reducing its sealing effectiveness. Conversely, a material with excessively high hardness would require the hydraulic actuation system to provide a substantially larger axial load. Therefore, HNBR with a Shore hardness of 70 was selected for elastomer seal. Based on the fitting results, the Ogden-3 model exhibits the best agreement with the uniaxial tensile stress–strain response, as illustrated in Figure 9. The fitted parameters are $mu_1 = 0.65394, \alpha_1 = -3.34274, mu_2 = 0.64877, \alpha_2 = -3.35286, mu_3 = 0.00228, \alpha_3 = 12.32987$. The remaining material properties used in the model are an elastic modulus of $E = 5.54\text{MPa}$ and a Poisson's ratio of $\mu = 0.495$.

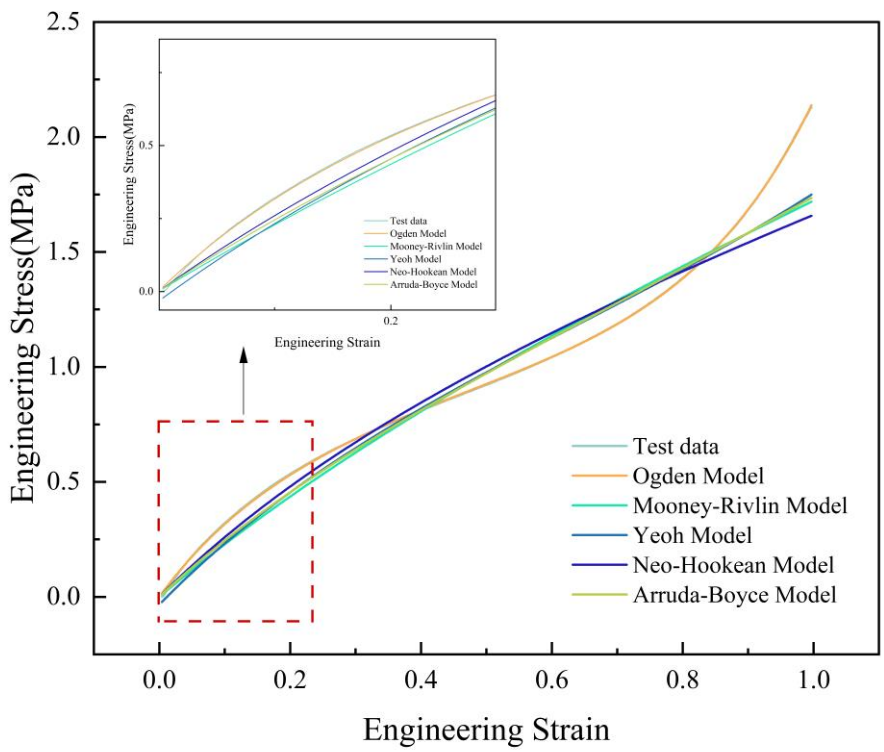

Figure 9 Fitting Results of the Uniaxial Tensile Data

4.2.4 Finite Element Model Setup

During emergency repair operations for subsea pipeline leakage, elastomer seal serves as the core component of the subsea pipeline plugging robot. Its primary functions are to seal the pipeline, isolate the internal oil and gas, and protect the structural integrity of the pipeline. Therefore, to accommodate the increasingly high pressures encountered in modern oil and gas pipelines, it is essential to further enhance the sealing performance of Elastomer seal.

To simulate the “self energisation” behavior of elastomer seal under internal fluid pressure, two analysis steps were defined. In the first step, the compression of elastomer seal driven by the hydraulic actuation system, during which full contact between elastomer seal and the pipe wall is established. In the second step, the internal fluid pressure is applied in conjunction with the pressure-penetration method to reproduce the operating condition corresponding to an internal pressure of 10 MPa within the pipeline.

(i) Boundary Conditions and Loading Conditions

The support cylinder, compression ring, fixing ring, and pipeline are all made of steel, ensuring high structural stability and collectively providing load-bearing support during operation. The fixing ring and the subsea pipeline are fully constrained, whereas the support cylinder is permitted to move freely in the radial direction and is fixed in all other degrees of freedom. The driving force is simulated using a uniformly distributed load, in which a uniform pressure of *P* MPa is applied to the inner surface of the hydraulic cylinder of the subsea pipeline plugging robot. The applied boundary conditions are illustrated in Figure 10. In Elastomer seal model examined in this study, the inner radius of the cartridge is $R_1 = 117mm$, the outer radius is $R_2 = 153mm$, and the inner radius of the pipeline is $R_3 = 163.5mm$.

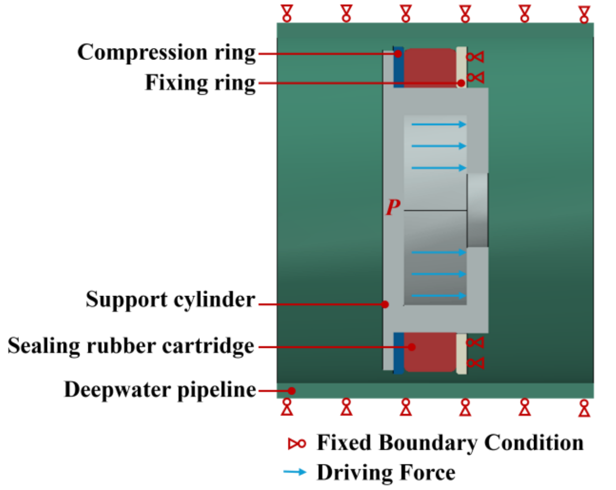

Figure 10 Application of Boundary Conditions

(ii) Contact Settings

In the finite element model, friction must be considered because contact occurs between multiple components. Therefore, friction coefficients were defined for all parts involved in the contact interactions. The corresponding contact parameters are summarized in Table 1.

Table 1 Contact Settings

Contact Name	Coefficient of Friction
Contact among the compression ring, fixing ring, and support cylinder	0.15
Contact between Elastomer seal and the compression ring, support cylinder, fixing ring, and pipe wall	0.30

(iii) Mesh-Independence Verification

In this study, eight-node linear hexahedral elements (C3D8R) were employed for the numerical simulations. The maximum stress values obtained for mesh sizes of 7 mm, 6 mm, 5 mm, 4 mm, and 3 mm were 230.5 MPa, 230.6 MPa, 249.4 MPa, 249.9 MPa, and 249.3 MPa, respectively. The results show a significant change in stress when the mesh is refined from 6 mm to 5 mm. However, further refinement from 5 mm to 3 mm produces only negligible variation in the computed stresses, indicating that a mesh size of 5 mm is sufficient to meet the accuracy requirements. Therefore, a mesh size of 5 mm was selected as the optimal configuration. The mesh-independence verification results are presented in Figure 11.

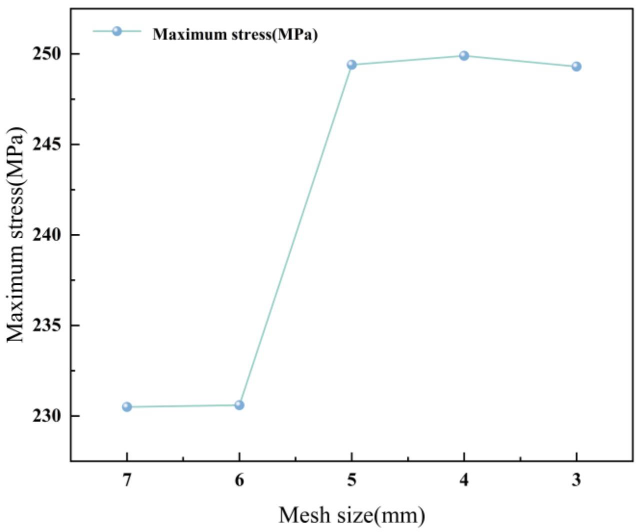

Figure 11 Mesh-Independence Verification

5 Numerical Analysis of the Sealing Performance

5.1 Analysis of the Self Energisation Characteristics of Elastomer Seal

Numerical simulation results show that when the hydraulic actuation load acting on elastomer seal is less than approximately 4 MPa, elastomer seal is unable to establish effective contact with the pipe wall. Once the hydraulic actuation load reaches 4 MPa, elastomer seal begins to contact the pipe wall and forms an initial seal. However, the ABAQUS pressure-penetration analysis indicates that the maximum contact stress generated at elastomer seal–pipe interface is only 9.495 MPa, which is insufficient to reliably seal an internal fluid pressure of 10 MPa.

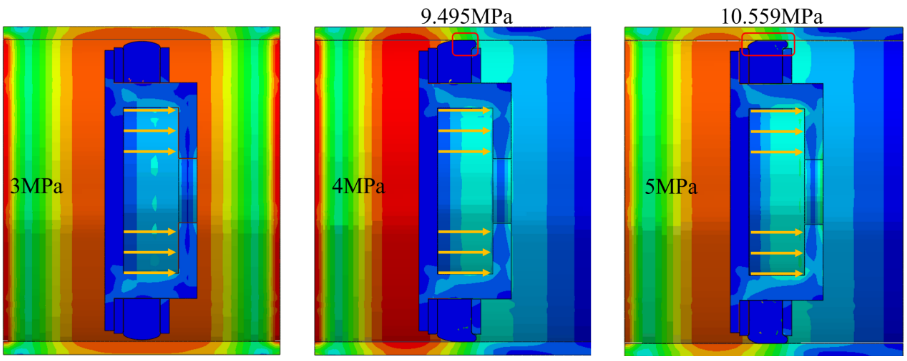

Figure 12 Schematic Illustration of the Self energisation Behavior of Elastomer seal

When the hydraulic actuation system of the subsea pipeline plugging robot continues to apply pressure to the cylinder until the hydraulic load reaches 5 MPa, elastomer seal establishes an initial seal with the pipe wall. At this stage, the average contact stress between elastomer seal and the pipe wall is approximately 1.038 MPa. Under the action of the internal fluid pressure, elastomer seal undergoes further compression, causing the contact pressure along the interface to increase progressively and ultimately reach 10.559 MPa. Therefore, the hydraulic actuation system of the plugging robot needs to apply only a 5 MPa cylinder pressure to achieve effective sealing against a 10 MPa internal fluid pressure, owing to the self energisation characteristic of elastomer seal, as illustrated in Figure 13.

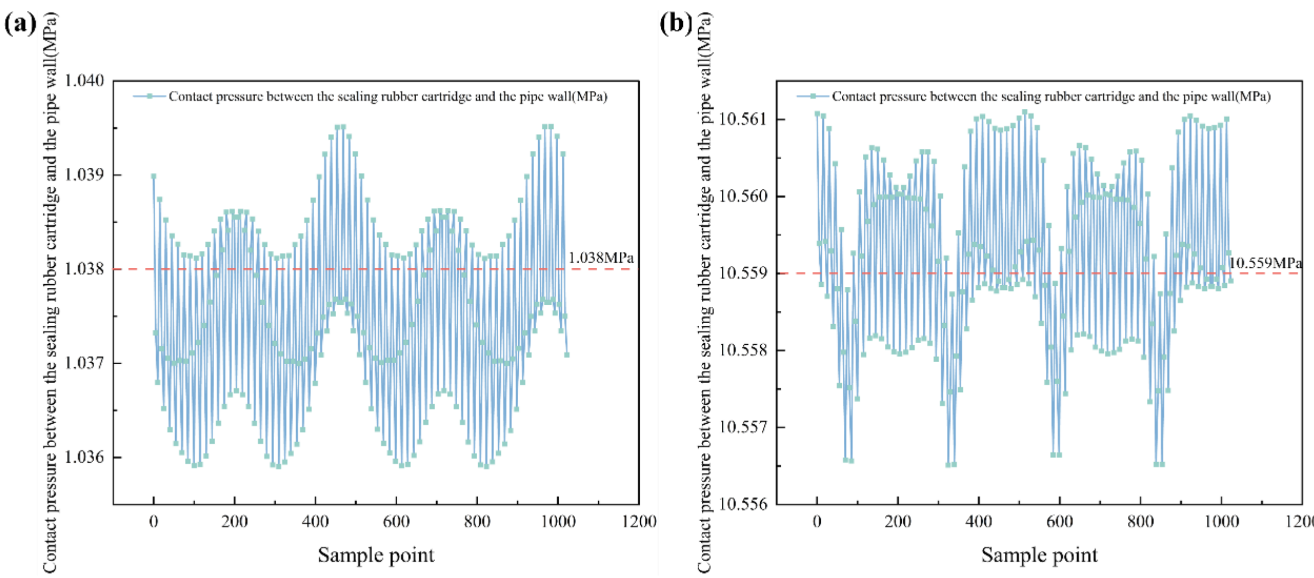

Figure 13 Contact Stress Curve Between Elastomer seal and the Pipe Wall Under a Hydraulic actuation Load of 5 MPa

5.2 Comparative Analysis of Numerical Simulation Results and Theoretical Calculations

A theoretical derivation of the contact stress between elastomer seal and the pipe wall was performed in this study, and the results were compared with those obtained from ABAQUS numerical simulations. As shown in Figure 14, the theoretical predictions exhibit good agreement with the finite-element results, indicating that the derived formulation can accurately describe the radial contact pressure generated during axial compression of elastomer seal. However, the theoretical values are slightly higher than the simulated results. This discrepancy primarily arises from two simplifying assumptions in the analytical model: (i) elastomer seal is assumed to remain incompressible during deformation, and (ii) outward extrusion of Elastomer seal is neglected. Although an anti-extrusion mechanism is incorporated in the actual structure, these theoretical assumptions are idealized, resulting in slightly higher predicted values.

When the hydraulic actuation load is below 172.787 kN, elastomer seal and the pipe wall are not yet in full contact, leading to a slightly larger deviation between the theoretical and simulated results. As the contact between elastomer seal and the pipe wall becomes more uniform and tighter, the discrepancy between the two methods correspondingly decreases. In this study, under medium-to-high hydraulic actuation loads, the minimum deviation between the theoretical predictions and the numerical simulation results is as small as 1.4%.

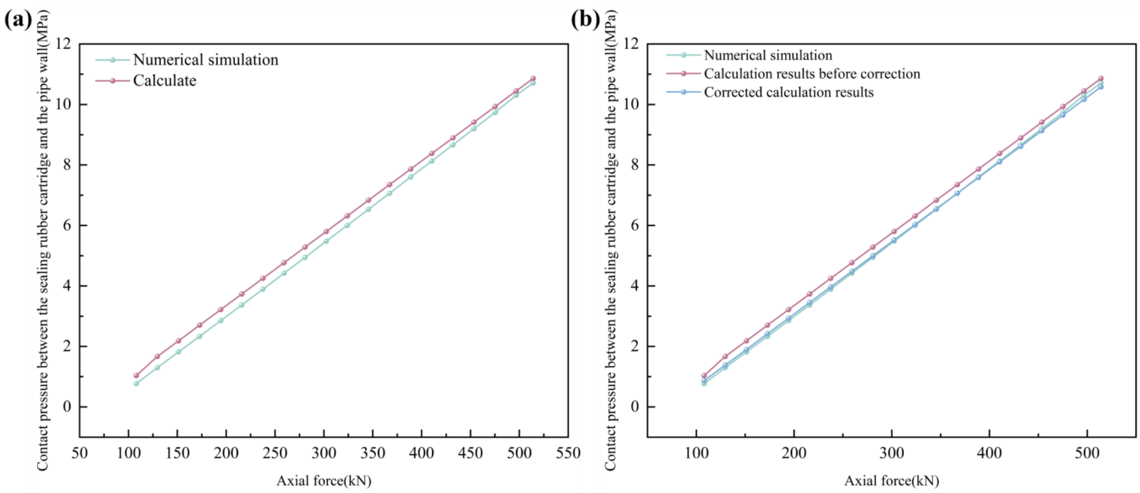

Figure 14 (a) Comparison Between the Theoretical Contact-Stress Expression and the Numerical Simulation Results During the Setting Stage; (b) Comparison After Applying the Corrected Theoretical Expression

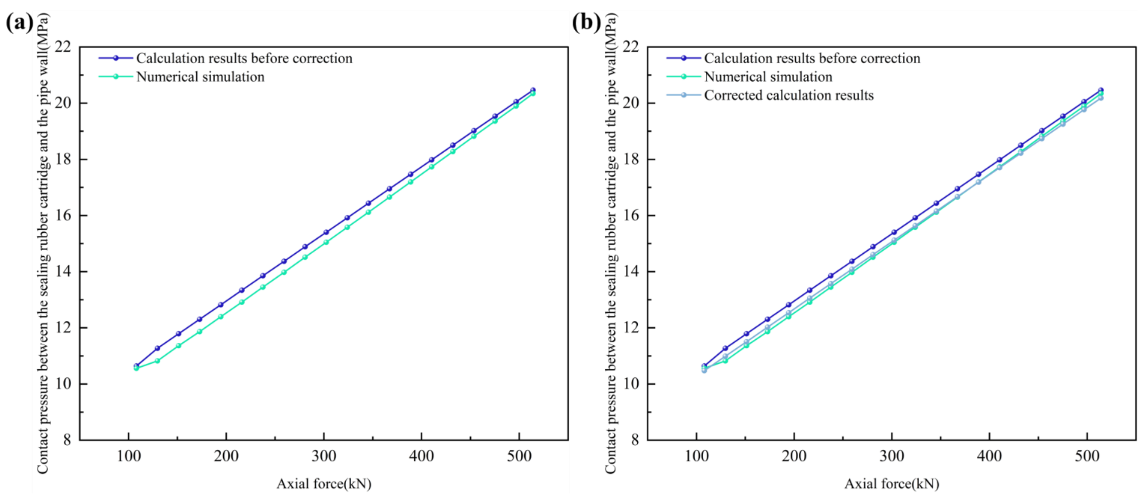

Figure 15 (a) Comparison Between the Theoretical Contact-Stress Expression and the Numerical Simulation Results During the Plugging Stage; (b) Comparison After Applying the Corrected Theoretical Expression

By comparing the results obtained from the two methods, the correction factor was determined to be $\varphi = 1.203$. After introducing this factor into the theoretical formulation, the modified equation can more accurately predict the contact stress between elastomer seal and the pipe wall under axial compression. Furthermore, during the plugging stage, the contact stress calculated using the corrected model shows good agreement with the numerical simulation results. Therefore, the corrected total contact stress between Elastomer seal and the pipe wall can be expressed as:

$$P = \frac{\mu F_z}{\pi(1-\mu)\left(R_3^2 - R_1^2\right)} - 1.203 * \frac{\mu E\left[\left(R_3^2 - R_1^2\right)^3 - \left(R_2^2 - R_1^2\right)^3\right]}{2\left(1-\mu^2\right)\left(R_2^2 - R_1^2\right)\left(R_3^2 - R_1^2\right)^2} + \frac{\mu \Delta P}{1-\mu}\left[1 - \frac{z}{2L}\left(\frac{R_3 - R_1}{R_3}\right)^2\right] \tag{39}$$

6 Conclusions

1) This study reviews the typical operational workflow of subsea pipeline plugging robot following a leakage event and analyzes the self energisation mechanism of elastomer seal under high-pressure internal fluids. The results demonstrate that an initial seal can be established when the hydraulic actuation system applies approximately 5 MPa of pressure to compress elastomer seal. Subsequently, driven by the internal fluid pressure, elastomer seal exhibits a "the higher the pressure, the tighter the seal" response, enabling reliable isolation of pipeline media at pressure levels up to 10 MPa.
2) A mechanical model of elastomer seal is developed, and a theoretical expression for the contact stress between elastomer seal and the pipe wall is derived.
3) The strain energy functions and nominal stress expressions under uniaxial tension for five commonly used hyperelastic constitutive models are systematically formulated, providing a theoretical foundation for identifying the rubber material parameters of elastomer seal.
4) The sealing performance of Elastomer seal under the setting load is numerically simulated using ABAQUS. In addition, the pressure-penetration method is employed to evaluate the contact stress distribution under the combined effects of the setting load and the internal fluid pressure.
5) A comparative analysis of theoretical predictions and numerical simulations is conducted, and the sources of their minor discrepancies are identified. Based on this comparison, the contact-stress formulation is further refined, allowing the corrected model to predict elastomer seal–pipe contact stress under hydraulic actuation with improved accuracy. The refined model offers a reliable analytical tool for the structural optimization and engineering design of subsea in-pipe plugging devices.

CRediT Authorship Contribution Statement

Mingkuan Wang: Investigation, Software, Validation, Visualization, Writing - original draft.

Enchao Zhang: Software, Writing - original draft. Shimin Zhang: Conceptualization, Methodology.

Shimin Zhang: Conceptualization, Methodology.

Xiaoxiao Zhu: Funding acquisition, Conceptualization, Writing - review & editing.

Declaration of Competing Interest

The authors declare that they have no known competing financial interests or personal relationships that could have appeared to influence the work reported in this paper.

References

[1] Zhu, X. X., Wang, M. K., Li, Y. T., Zhang, S. M., Zhang, L. B., 2024. Research on key technologies and equipment for emergency response to oil and gas pipeline leaks. Pipeline Protection 1, 12-19. https://doi.org/10.26949/j.issn.2097-5260.2024.01.002

[2] Zhu, X., Wang, H., Li, F., Quan, Y., Wang, W., Zhang, S., 2017. Research on the automatically trajectory control of a spherical isolation plug in subsea pipeline. Ocean Engineering 141, 101-107. https://doi.org/10.1016/j.oceaneng.2017.06.025

[3] Min, Z. S., Min, L. Y., Ming, M. Y., Wen, F. B., 2009. Intelligent plugging techniques in high-pressure pipeline. Oil & Gas Storage and Transportation 28, 59-61+79+87. https://doi.org/10.6047/j.issn.1000-8241.2009.06.017

[4] Fan, W. B., Zhang, S. M., 2008. Design of high-pressure intelligent plug in pipe. China Petroleum Machinery, 213-215. https://doi.org/10.16082/j.cnki.issn.1001-4578.2008.09.055

[5] TDW. Smart Plug® pipeline isolation system [EB/OL]. 2013-3-20 [2013-12-04]. http://www.tdwilliaamson.com/en/Services/HotTapping/smartplugonshore/Pages/home.aspx

[6] Stats group. Process & Pipeline Isolation: Tecno Plug™ [EB/OL]. 2012-05-12 [2013-12-04]. http://www.statsgroup.com/PipelineIsolation/PipelineIsolationTecnoPlug.html

[7] Zhang, Z., Zhu, X. H., Xu, J. B., 2019. Structural parameters optimization of compression packer rubber based on orthogonal test. Natural Gas Industry 39, 80-84. https://doi.org/10.3787/j.issn.1000-0976.2019.03.010

[8] Li, B., Lv, D. W., Zhang, Z. P., 2018. Analysis of mechanical properties of wave packer rubber. Chinese Journal of Applied Mechanics 35, 828-833+935. https://doi.org/10.11776/cjam.35.04.B026

[9] Liang, H., Guo, Z. L., Wang, X. L., He, F. G., Wu, C. H., Li, W. B., 2023. Extrusion failure analysis and improved design of sealing structure of packer. Chinese Hydraulics & Pneumatics 47, 177-182. https://doi.org/10.11832/j.issn.1000-4858.2023.07.022

[10] Zhang, K., Wu, K., 2022. Parameter optimization of the sealing performance of the rubber packer inside pipeline based on ABAQUS. Oil Field Equipment 51, 45-52. https://doi.org/10.3969/j.issn.1001-3482.2022.01.006

[11] Xu, J., Ma, L., Yang, J. L., Han, C., Cao, F., 2025. Sealing performance of dual tubing packer rubber in branch holes. Oil Field Eouipment 54, 35-40. https://doi.org/10.3969/j.issn.1001-3482.2025.04.005

[12] Hu, G., Zhang, P., Wang, G. R., Zhang, M., Li, M., 2017. The influence of rubber material on sealing performance of packing element in compression packer. Journal of Natural Gas Science and Engineering 38, 120-138. https://doi.org/10.1016/j.jngse.2016.12.027

[13] Sun, Q. L., Xia, L., Liu, Y. W., Feng, D., Hou, L. X., Deng, L., 2024. Performance analysis of packer rubber tube under closed annulus pressure variation in deep water test. Lubrication Engineering 49, 147-153. https://doi.org/10.3969/j.issn.0254-0150.2024.04.020

[14] Chen, Y., Liu, X., Li, C., 2022. Development of rubber packing element for 105 MPa/215°C deep-well test packer. Materials 15, 2024. https://doi.org/10.3390/MA15062024

[15] Wang, P. C., Chen, M. H., Jenkinson, J., Song, Y. X., Sun, L., 2024. Interfacial friction effects on sealing performances of elastomer packer. Petroleum Science 21, 2037-2047. https://doi.org/10.1016/j.petsci.2023.11.015

[16] He, Y. X., Ma, H. Y., Tan, X. B., Chen, L., Wan, J. F., Yue, R. C., Yi, X. Z., 2025. Mechanical properties and sealing performance evaluation of packers in high temperature underground gas storage. Scientific Reports 15, 20925. https://doi.org/10.1038/S41598-025-02496-9

[17] Polonsky, V. L., Tyurin, A. P., 2015. Design of packers for sealing of the inter-tube space in equipment used for recovery of oil and gas. Chemical and Petroleum Engineering 51, 37-40. https://doi.org/10.1007/s10556-015-9994-2

[18] Zhu, Z. K., Cai, M., Cui, L. N., Song, X. L., Xu, X. Y., Cong, C. B., Li, H. C., Gao, Q. M., 2024. Simulation of the static sealing performance of rubber packer cylinders in a supercritical–CO_2 environment. Energies 17, 3305. https://doi.org/10.3390/EN17133305

[19] Li, J. H., Wu, C. H., Li, M. J., Wang, C. W., 2024. Study on sealing performance of spring-embedded shoulder protection packer rubber cylinder. Processes 12, 1967. https://doi.org/10.3390/PR12091967

[20] Zhang, Y. W., Wang, H. X., Che, J. Q., Du, M. C., Zhang, H. J., 2021. Multi-objective optimization and experiment of nylon cord rubber in expandable packer. Petroleum Science 18, 269-284. https://doi.org/10.1007/s12182-020-00539-6

[21] Fei, G. S., Zheng, X., Zhao, C. Q., 2025. Study on seal leakage test and simulation analysis of packer at high temperature and high pressure. Journal of Petroleum Exploration and Production Technology 15, 1-15. https://doi.org/10.1007/S13202-025-02072-X

[22] Song, M. H., Wang, W., Sun, C., 2025. Numerical simulation and structural optimisation of sealing performance for rubber packers. Journal of Rubber Research 28, 211-222s215. https://doi.org/10.1007/S42464-025-00299-1

[23] Li, C., Guan, Z. C., Zhang, B., Wang, Q., Xie, H. Q., Yan, Y., Han, C., 2021. Failure and mitigation study of packer in the subsea HTHP gas well considering the temperature-pressure effect during well completion test. Case Studies in Thermal Engineering 26, 101021. https://doi.org/10.1016/J.CSITE.2021.101021

[24] ABAQUS: Theory manual: Version 6.10 [M]. Providence: Hibbitt, Karlsonn and Sorensen, Inc., 2010.

[25] Mlyniec, A., Morawska-Chochol, A., Kloch, K., Uhl, T., 2014. Phenomenological and chemomechanical modeling of the thermomechanical stability of liquid silicone rubbers. Polymer Degradation and Stability 99, 290-297. https://doi.org/10.1016/j.polymdegradstab.2013.10.018

[26] Ogden, R. W., 1973. Large deformation isotropic elasticity—on the correlation of theory and experiment for incompressible rubberlike solids. Rubber Chemistry and Technology 46, 398-416. https://doi.org/10.1098/rspa.1972.0096

[27] Yeoh, O. H., 1990. Characterization of elastic properties of carbon-black-filled rubber vulcanizates. Rubber Chemistry and Technology 63, 792-805. https://doi.org/10.5254/1.3538289

[28] Arruda, E. M., Boyce, M. C., 1993. A three-dimensional constitutive model for the large stretch behavior of rubber elastic materials. Journal of the Mechanics and Physics of Solids 41, 389-412. https://doi.org/10.1016/0022-5096(93)90013-6

[29] Hassani, R., Ansari, R., Rouhi, H., 2019. Large deformation analysis of 2D hyperelastic bodies based on the compressible nonlinear elasticity: A numerical variational method. International Journal of Non-Linear Mechanics 116, 39-54. https://doi.org/10.1016/j.ijnonlinmec.2019.05.003